Inversion of azimuthal seismic amplitude differences for tilted fracture weaknesses

Huaizhen Chen* and Kristopher A. Innanen

ABSTRACT

Based on the linear slip fracture model, we first express stiffness matrix of tilted transversely isotropic (TTI) media in terms of the normal and tangential fracture weaknesses. Using perturbations in stiffness parameters for the case of an interface separating an isotropic medium and a TTI medium, we derive a linearized P-to-P reflection coefficient as a function of fracture weaknesses, in which titled fracture weaknesses involving effects of tilt angle and fracture weaknesses emerge. Following a Bayesian framework, we propose an inversion approach to use amplitude differences between seismic data along two azimuths to estimate the tangential fracture weakness and tilted normal and tangential fracture weaknesses based on the derived and simplified reflection coefficient. Synthetic tests confirm that the unknown parameter vector involving the tangential fracture weakness and tilted fracture weaknesses is estimated stably and reliably in the case of seismic data containing a moderate Gaussian noise. The inversion approach is also applied to a field data set acquired from a fractured carbonate reservoir, from which reasonable results of tilted fracture weaknesses are obtained. We conclude that the proposed inversion approach may provide additional proofs for fracture characterization, and it also make the estimation of tilt angle from observed seismic data for fractured reservoirs be available.

INTRODUCTION

Seismic wave propagation in most subsurface layers exhibits phenomenon of anisotropy. Transversely isotropic (TI) model plays a important role in characterization of seismic wave propagation in anisotropic media (Alkhalifah and Larner, 1994; Alkhalifah, 1995; Grechka et al., 2001; Bakulin et al., 2010; Wang and Tsvankin, 2013). Rocks containing a set of parallel vertical fractures is equivalent to horizontal transversely isotropic (HTI) media (Schoenberg and Douma, 1988; Schoenberg and Sayers, 1995; Bakulin et al., 2000; Chen et al., 2014), and finely layered rocks with a vertical symmetry axis are assumed to be vertical transversely isotropic (VTI) media (Thomsen, 1986; Carcione, 1992; Berryman et al., 1999; Carcione, 2000; Stovas et al., 2006). Moreover, TI media with a tilted symmetry axis are named tilted TI (TTI) media, which are usually formed by rotating HTI media or VTI media (Behera and Tsvankin, 2009; Fletcher et al., 2009; Nadri et al., 2012; Stovas and Alkhalifah, 2013; Wang and Tsvankin, 2013; Wang and Peng, 2015; Shragge, 2016). In the present study, we focus on the TTI media formed by rotating the vertically fractured rocks (i.e. rocks containing a set of parallel fractures with a tilted symmetry axis).

Zoeppritz formula is proposed to describe how seismic wave energy partitions at a reflection interface, which is well applied to measure exact reflection and transmission coefficients of seismic wave (Shuey, 1985; Sheriff and Geldart, 1995; Aki and Richards, 2002; Avseth et al., 2010), and it has been extended to weakly anisotropic media to compute exact solutions of seismic wave transmission and reflection coefficients (Schoenberg and Protázio, 1992; Rüger, 1996; Pšenčík and Vavryčuk, 1998). Quantities required

to compute exact solutions of reflection coefficients in weakly anisotropic media involve polarization vectors and azimuthal angles (Thomsen, 1988; Tsvankin, 1997; Pšenčík and Gajewski, 1998); however, the complexity of Zoeppritz formula restricts its application in the calculation of reflection coefficients and the inversion of observed seismic data, which makes the derivation of a linearized reflection coefficient for TTI media be our first goal.

Hudson (1980) proposed an effective model to study how penny-shaped cracks affect stiffness matrix of anisotropic rocks. In the case of rocks containing a set of vertical and rotationally invariant fractures, a linear slip model is established to characterize influences of fractures on total properties of rocks as a function of the normal and tangential fracture weaknesses (Schoenberg and Douma, 1988; Schoenberg and Sayers, 1995). Combining the penny-shaped crack model and the linear slip model, Bakulin et al. (2000) related the normal and tangential fracture weaknesses to fracture properties (fracture density and aspect ratio). In order to implement seismic inversion for fracture weaknesses and fracture tilt angle, we will derive the derived reflection coefficient of P-wave incidence and P-wave reflection (P-to-P) in terms of tilted fracture weaknesses based on the linear slip model.

In this study, using the stiffness matrix of HTI media given by the linear slip model, we first express the stiffness matrix of TTI media in terms of tilted fracture weaknesses. Using perturbations in stiffness parameters and relationship between scattering function and reflection coefficients, we obtain the P-to-P linearized reflection coefficient a function of tilted fracture weaknesses. Base on the derived reflection coefficient, we demonstrate an inversion approach to employ amplitude differences between seismic data along different azimuths to estimate tilted fracture weaknesses. We testify the stability and robustness of the proposed inversion using synthetic seismic data in which random noise are added, and applying the proposed approach to a real data set, we confirm that our approach may generate valuable and meaningful results for detecting fractures and computing fracture tilt angles.

THEORY AND METHOD

Stiffness matrix related to tilted fracture weaknesses

The stiffness matrix of TTI medium, $\mathbf{C}_{\text{TTI}}$, is expressed using the stiffness matrix of corresponding VTI medium, $\mathbf{C}_{\text{VTI}}$, which is given by (Auld, 1990)

$$\mathbf{C}_{\text{TTI}} = \mathbf{M}_\nu \mathbf{C}_{\text{VTI}} \mathbf{M}_\nu^T, \tag{1}$$

where

$$\mathbf{M}_\nu = \begin{bmatrix} \cos^2\nu & 0 & \sin^2\nu & 0 & -\sin 2\nu & 0 \\ 0 & 1 & 0 & 0 & 0 & 0 \\ \sin^2\nu & 0 & \cos^2\nu & 0 & \sin 2\nu & 0 \\ 0 & 0 & 0 & \cos\nu & 0 & \sin\nu \\ \frac{1}{2}\sin 2\nu & 0 & -\frac{1}{2}\sin 2\nu & 0 & \cos 2\nu & 0 \\ 0 & 0 & 0 & -\sin\nu & 0 & \cos\nu \end{bmatrix}, \tag{2}$$

and $\mathbf{M}_\nu^T$ is the transpose of $\mathbf{M}_\nu$, ν denotes the tilt angle, which indicates the angle between the symmetry axis and the z axis, as plotted in Figure 1. In the case of ν being 90°, the TTI medium becomes HTI medium, and when ν is equal to 0°, the TTI medium becomes VTI medium. For the TTI medium, which is equivalent of a rock containing a set of parallel fractures with a tilted symmetry axis, we first express stiffness matrix of corresponding

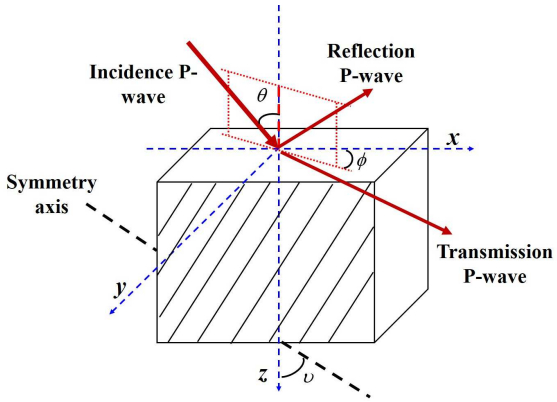

FIG. 1. P-wave propagation in tilted transversely isotropic media. Quantities θ and ϕ are incidence angle of P-wave and azimuthal angle of observation, respectively.

VTI medium using the stiffness matrix of HTI medium proposed by the linear slip model. Given a tilt angle, we may derive stiffness parameters of TTI medium in terms of fracture weaknesses. In the linear slip model, the stiffness matrix of HTI medium is given by (Schoenberg and Douma, 1988; Schoenberg and Sayers, 1995; Gurevich, 2003)

$$\mathbf{C}_{\mathrm{HTI}} = \begin{bmatrix} M(1-\delta_N) & \lambda(1-\delta_N) & \lambda(1-\delta_N) & 0 & 0 & 0 \\ \lambda(1-\delta_N) & M\left(1-\chi^2\delta_N\right) & \lambda(1-\chi\delta_N) & 0 & 0 & 0 \\ \lambda(1-\delta_N) & \lambda(1-\chi\delta_N) & M\left(1-\chi^2\delta_N\right) & 0 & 0 & 0 \\ 0 & 0 & 0 & \mu & 0 & 0 \\ 0 & 0 & 0 & 0 & \mu(1-\delta_T) & 0 \\ 0 & 0 & 0 & 0 & 0 & \mu(1-\delta_T) \end{bmatrix}, \tag{3}$$

where $M = \lambda + 2\mu$, λ and μ are Lamé constants of the homogeneous isotropic host rock, $\chi = \lambda/M$, and δ_N and δ_T are the normal and tangential fracture weaknesses, which are related to fracture properties (e.g. fracture density and filling fluid moduli). Letting the tilt angle ν be 90° and $\mathbf{C}_{\mathrm{TTI}}$ be equal to $\mathbf{C}_{\mathrm{HTI}}$, we use equation 1 to express the stiffness matrix of corresponding VTI medium as

$$\mathbf{C}_{\mathrm{VTI}} = \left(\mathbf{M}_{\nu=90^\circ}\right)^{-1} \mathbf{C}_{\mathrm{HTI}} \left(\mathbf{M}^T_{\nu=90^\circ}\right)^{-1}, \tag{4}$$

where $\left(\mathbf{M}_{\nu=90^\circ}\right)^{-1}$ and $\left(\mathbf{M}^T_{\nu=90^\circ}\right)^{-1}$ are inverse matrices of $\mathbf{M}_{\nu=90^\circ}$ and $\mathbf{M}^T_{\nu=90^\circ}$ respectively. Combining equations 1-4, we derive the stiffness matrix of TTI medium in terms of fracture weaknesses

$$\mathbf{C}_{\mathrm{TTI}} = \begin{bmatrix} C_{11} & C_{12} & C_{13} & 0 & C_{15} & 0 \\ C_{12} & C_{22} & C_{23} & 0 & C_{25} & 0 \\ C_{13} & C_{23} & C_{33} & 0 & C_{35} & 0 \\ 0 & 0 & 0 & C_{44} & 0 & C_{46} \\ C_{15} & C_{25} & C_{35} & 0 & C_{55} & 0 \\ 0 & 0 & 0 & C_{46} & 0 & C_{66} \end{bmatrix} = \mathbf{M}_\nu \left(\mathbf{M}_{\nu=90^\circ}\right)^{-1} \mathbf{C}_{\mathrm{HTI}} \left(\mathbf{M}^T_{\nu=90^\circ}\right)^{-1} \mathbf{M}^T_\nu, \tag{5}$$

where

$$\begin{aligned} C_{11} =& M\left(1-\chi^2\delta_N\right)\cos^4\nu + \frac{1}{2}\lambda\left(1-\delta_N\right)\left(\sin 2\nu\right)^2 \\ &+ M\left(1-\delta_N\right)\sin^4\nu + \mu\left(1-\delta_T\right)\left(\sin 2\nu\right)^2, \end{aligned}$$

$$C_{12} = \lambda\left(1-\chi\delta_N\right)\cos^2\nu + \lambda\left(1-\delta_N\right)\sin^2\nu,$$

$$
\begin{aligned}
C_{13} =& \frac{1}{4}M\left(1-\chi^2\delta_N\right)\left(\sin 2\nu\right)^2+\lambda\left(1-\delta_N\right)\sin^4\nu+\lambda\left(1-\delta_N\right)\cos^4\nu \\
&+\frac{1}{4}M\left(1-\delta_N\right)\left(\sin 2\nu\right)^2-\mu\left(1-\delta_T\right)\left(\sin 2\nu\right)^2, \\
C_{15} =& M\left(1-\chi^2\delta_N\right)\sin\nu\cos^3\nu-\lambda\left(1-\delta_N\right)\sin\nu\cos^3\nu \\
&-2\mu\left(1-\delta_N\right)\sin^3\nu\cos\nu-\mu\left(1-\delta_T\right)\sin 2\nu\cos 2\nu, \\
C_{22} =& M\left(1-\chi^2\delta_N\right), \\
C_{23} =& \lambda\left(1-\chi\delta_N\right)\sin^2\nu+\lambda\left(1-\delta_N\right)\cos^2\nu, \\
C_{25} =& \lambda\left(1-\chi\delta_N\right)\left(\frac{1}{2}\sin 2\nu\right)-\lambda\left(1-\delta_N\right)\left(\frac{1}{2}\sin 2\nu\right), \\
C_{33} =& M\left(1-\chi^2\delta_N\right)\sin^4\nu+\frac{1}{2}\lambda\left(1-\delta_N\right)\left(\sin 2\nu\right)^2+M\left(1-\delta_N\right)\cos^4\nu, \\
C_{35} =& M\left(1-\chi^2\delta_N\right)\sin^3\nu\cos\nu-\lambda\left(1-\delta_N\right)\sin^3\nu\cos\nu \\
&-2\mu\left(1-\delta_N\right)\sin\nu\cos^3\nu+\mu\left(1-\delta_T\right)\cos 2\nu\sin 2\nu, \\
C_{44} =& \mu-\mu\delta_T\cos^2\nu, C_{46}=\mu\delta_T\sin\nu\cos\nu, \\
C_{55} =& \frac{1}{4}M\left(1-\chi^2\delta_N\right)\left(\sin 2\nu\right)^2+\frac{1}{4}M\left(1-\delta_N\right)\left(\sin 2\nu\right)^2 \\
&-\frac{1}{2}\lambda\left(1-\delta_N\right)\left(\sin 2\nu\right)^2+\mu\left(1-\delta_T\right)\left(\cos 2\nu\right)^2, \\
C_{66} =& \mu-\mu\delta_T\sin^2\nu.
\end{aligned}
\tag{6}
$$

Derivation of P-to-P reflection coefficient for TTI media

Using the derived stiffness matrix, we next express perturbations in stiffness parameters in the case of one interface separating an isotropic layer and a TTI layer. The perturbation in stiffness matrix is given by

$$
\Delta\mathbf{C}_{\text{TTI}}=\begin{bmatrix}
\Delta C_{11} & \Delta C_{12} & \Delta C_{13} & 0 & \Delta C_{15} & 0 \\
\Delta C_{12} & \Delta C_{22} & \Delta C_{23} & 0 & \Delta C_{25} & 0 \\
\Delta C_{13} & \Delta C_{23} & \Delta C_{33} & 0 & \Delta C_{35} & 0 \\
0 & 0 & 0 & \Delta C_{44} & 0 & \Delta C_{46} \\
\Delta C_{15} & \Delta C_{25} & \Delta C_{35} & 0 & \Delta C_{55} & 0 \\
0 & 0 & 0 & \Delta C_{46} & 0 & \Delta C_{66}
\end{bmatrix}, \tag{7}
$$

where

$$
\begin{aligned}
\Delta C_{11}\approx& \left(4\mu\cos^4\nu-4\mu\cos^2\nu\right)\delta_T+\left[\left(-M\chi^2+M-4\mu\right)\cos^4\nu+4\mu\cos^2\nu-M\right]\delta_N+\Delta M, \\
\Delta C_{12}\approx& \left[-\left(\chi-1\right)\left(M-2\mu\right)\cos^2\nu-M+2\mu\right]\delta_N-2\Delta\mu+\Delta M, \\
\Delta C_{13}\approx& \left[\left(M\chi^2-M+4\mu\right)\cos^4\nu+\left(-M\chi^2+M-4\mu\right)\cos^2\nu-M+2\mu\right]\delta_N \\
&+\left(-4\mu\cos^4\nu+4\mu\cos^2\nu\right)\delta_T+\Delta M-2\Delta\mu, \\
\Delta C_{15}\approx& -\frac{1}{2}\sin 2\nu\left[\left(M\chi^2-M+4\mu\right)\cos^2\nu-2\mu\right]\delta_N-\sin 2\nu\left(-2\mu\cos^2\nu+\mu\right)\delta_T, \\
\Delta C_{22}\approx& -M\chi^2\delta_N+\Delta M,
\end{aligned}
$$

$$\Delta C_{23}\approx\left[(\chi-1)(M-2\mu)\cos^2\nu-\chi(M-2\mu)\right]\delta_N+\Delta M-2\Delta\mu,$$

$$\Delta C_{25}\approx\frac{1}{2}(M-2\mu)(\chi-1)\sin 2\nu\delta_N,$$

$$\begin{aligned}\Delta C_{33}\approx&\left[\left(-M\chi^2+M-4\mu\right)\cos^4\nu+\left(2M\chi^2-2M+4\mu\right)\cos^2\nu-M\chi^2\right]\delta_N\\&+\left(4\cos^4\nu-4\cos^2\nu\right)\Delta\mu+4\mu\cos^4\nu-4\mu\cos^2\nu+\Delta M,\end{aligned}$$

$$\Delta C_{35}\approx\frac{1}{2}\sin 2\nu\left[\left(M\chi^2-M+4\mu\right)\cos^2\nu-M\chi^2+M-2\mu\right]\delta_N+\sin 2\nu\left(-2\mu\cos^2\nu+\mu\right)\delta_T,$$

$$\Delta C_{44}\approx\Delta\mu-\mu\cos^2\nu\delta_T,\ \Delta C_{46}\approx\frac{1}{2}\mu\sin 2\nu\delta_T,$$

$$\Delta C_{55}\approx\left[\left(\frac{M}{4}\chi^2-M+4\mu\right)(\cos 2\nu)^2-\frac{M}{4}\chi^2+\frac{M}{4}-\mu\right]\delta_N-\mu(\cos 2\nu)^2\delta_T+\Delta\mu,$$

$$\Delta C_{66}\approx\left(\mu\cos^2\nu-\mu\right)\delta_T+\Delta\mu. \tag{8}$$

It is important to stress that in the derivation of perturbations in stiffness parameters, we neglect the term proportional to $\Delta M\delta_N$, $\Delta\mu\delta_N$, $\Delta M\delta_T$ and $\Delta\mu\delta_T$ under the assumptions of small changes in elastic properties of host rock across the interface and weak fracture weaknesses. The relationship between P-to-P reflection coefficient and perturbations in stiffness parameters is given by (Shaw and Sen, 2006; Chen et al., 2018)

$$R_{\mathrm{PP}}=\frac{1}{4\rho\cos^2\theta}\begin{bmatrix}\Delta\rho\cos 2\theta+\Delta C_{11}\xi_{11}+\Delta C_{12}(\xi_{12}+\xi_{21})+\Delta C_{13}(\xi_{13}+\xi_{31})\\+\Delta C_{15}(\xi_{15}+\xi_{51})+\Delta C_{22}\xi_{22}+\Delta C_{23}(\xi_{23}+\xi_{32})+\\\Delta C_{25}(\xi_{25}+\xi_{52})+\Delta C_{33}\xi_{33}+\Delta C_{35}(\xi_{35}+\xi_{53})+\Delta C_{44}\xi_{44}\\+\Delta C_{46}(\xi_{46}+\xi_{64})+\Delta C_{55}\xi_{55}+\Delta C_{66}\xi_{66}\end{bmatrix}, \tag{9}$$

where ξ_{ij} is related to P-wave incidence angle θ and observation azimuth ϕ (Shaw and Sen, 2006). Substituting equation 8 into equation 9, we obtain a P-to-P linearized reflection coefficient for the interface separating an isotropic layer and a TTI layer as

$$\begin{aligned}R_{\mathrm{PP}}(\theta,\phi)=&\frac{1}{2}\sec^2\theta\left(\frac{\Delta M}{2M}\right)-\left(4\sin^2\theta+2\cos^2\nu-2\cos^4\nu\right)\left(\frac{\Delta\mu}{2\mu}\right)\\&+\frac{1}{2}\frac{\cos 2\theta}{\cos^2\theta}\left(\frac{\Delta\rho}{2\rho}\right)-\begin{bmatrix}\frac{1}{4}\sec^2\theta(1-2g)^2+g(1-2g)\tan^2\theta\cos^2\phi\\+g^2\cos^2\theta\cos^4\nu-g(1-2g)\tan^2\theta\cos^2\phi\cos^2\nu\\g(1-2g)\cos^2\nu+g^2\sin^2\theta\tan^2\theta\cos^4\phi\sin^4\nu\end{bmatrix}\delta_N\\&+g\begin{bmatrix}2\sin^2\theta\cos^2\phi-\tan^2\theta\cos^2\phi\\2\sin^2\theta\cos^2\phi\cos^4\nu+\sin^2\theta\tan^2\theta\cos^4\phi\sin^4\nu\\-4\sin^2\theta\cos^2\phi\cos^2\nu+\tan^2\theta\cos^2\phi\cos^2\nu+\sin^2\theta\cos^2\nu\end{bmatrix}\delta_T,\end{aligned} \tag{10}$$

where $g=\mu/M$, and $\Delta M/(2M)$, $\Delta\mu/(2\mu)$ and $\Delta\rho/(2\rho)$ are reflectivities of P- and S-wave moduli and density, respectively. We observe that the effect of tilt angle on the reflection coefficient is coupled with effects of S-wave modulus reflectivity and fracture weaknesses.

We next simplify the derived reflection coefficient and analyze the effect of tilt angle on reflection coefficient. Under the assumption that the P-wave incidence angle is less than 30°, we neglect the term proportional to $\sin^2\theta\tan^2\theta$, and in the case that the set of parallel

fractures has a relatively high tilt angle, we neglect the term proportional to $\cos^4\nu$. The reflection coefficient is simplified to

$$\begin{aligned} R_{\rm PP}(\theta,\phi)\approx&\frac{1}{4}\sec^2\theta\frac{\Delta M}{M}-(1+2\sin^2\theta)\frac{\Delta\mu}{\mu}+\frac{1}{4}\frac{\cos 2\theta}{\cos^2\theta}\frac{\Delta\rho}{\rho}\\ &-\frac{1}{4}(1-2g)\left[(1-2g)\sec^2\theta+4g\right]\delta_N-g\sin^2\theta\cos 2\phi\delta_T\\ &+\delta_{\nu\mu}+g(1-2g)(1-\tan^2\theta\cos^2\phi)\delta_{\nu N}\\ &+\left(4g\sin^2\theta\cos^2\phi-g\tan^2\theta\cos^2\phi-g\sin^2\theta\right)\delta_{\nu T}, \end{aligned} \tag{11}$$

where $\delta_{\nu\mu}=\sin^2\nu\Delta\mu/\mu$, $\delta_{\nu N}=\sin^2\nu\delta_N$ and $\delta_{\nu T}=\sin^2\nu\delta_T$, which are named tilted S-wave modulus reflectivity and fracture weaknesses, respectively. We next compare the reflection coefficients calculated using equations 10 and 11 to verify the accuracy of the simplified reflection coefficient. Figure 2 shows a model of an interface formed by involving a set of tilted fractures into a rock. In the case that tilted fractures are filled with gas, we plot variations of reflection coefficient with fracture density e, incidence angle θ and tilt angle ν in Figure 3. We observe that differences between the reflection coefficients calculated using equations 10 and 11 respectively increase with P-wave incidence angle and fracture density, and decreases as the tilt angle increases, which indicates the simplified reflection coefficient (equation 11) is applicable in gas-saturated fractured reservoirs those have a small fracture density and a high tilt angle, and the accuracy of the simplified reflection coefficient is also confirmed in the case of the incidence angle being less than $30°$.

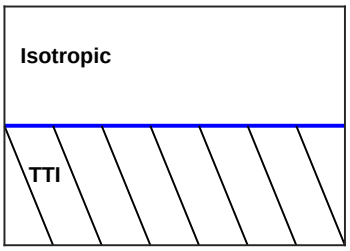

FIG. 2. A model of an interface separating an isotropic layer and a TTI layer.

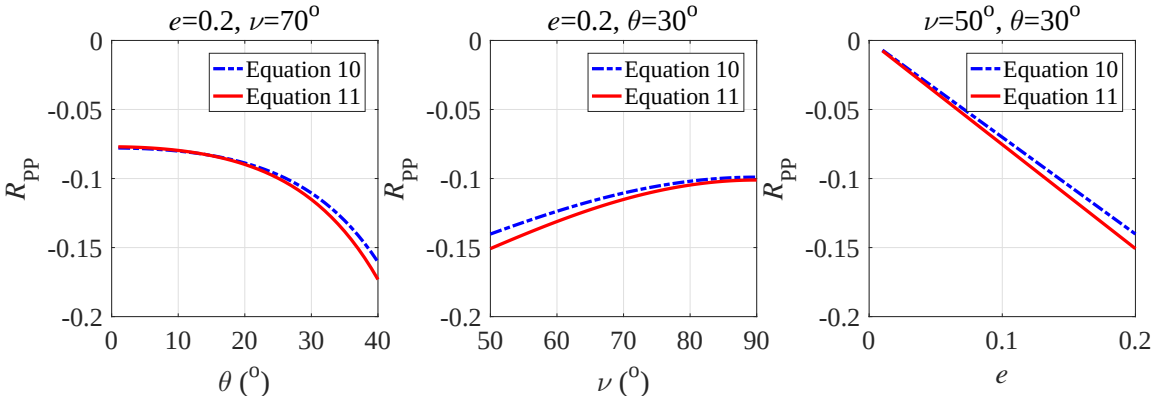

FIG. 3. Variations of reflection coefficients with fracture density e, P-wave incidence angle θ and tilt angle ν. S-to-P wave moduli ratio g is 0.25.

Azimuthal seismic inversion for tangential fracture weaknesses and tilted fracture weaknesses

We proceed to the estimation of tangential fracture weakness and tilted fracture weaknesses from amplitude differences among seismic data at different azimuthal angles. Based on the simplified reflection coefficient, we first express the difference between reflection coefficients at two azimuthal angles (ϕ_1 and ϕ_2)

$$\begin{aligned}\Delta R_{\rm PP} =& R_{\rm PP}(\theta,\phi_2) - R_{\rm PP}(\theta,\phi_1)\\ =& -g\sin^2\theta\left(\cos 2\phi_2 - \cos 2\phi_1\right)\delta_T\\ &-g(1-2g)\tan^2\theta\left(\cos^2\phi_2-\cos^2\phi_1\right)\delta_{\nu N}\\ &+g(4\sin^2\theta-\tan^2\theta)(\cos^2\phi_2-\cos^2\phi_1)\delta_{\nu T}.\end{aligned} \tag{12}$$

We observe that the difference between azimuthal reflection coefficients is influenced by the tangential fracture weaknesses and tilted fracture weaknesses. We next study how the normal and tangential fracture weaknesses affect the difference between azimuthal reflection coefficients in TTI media. Given different fracture weaknesses and tilt angles, we plot variations of differences between azimuthal reflection coefficients with P-wave incidence angle, as plotted in Figure 4.

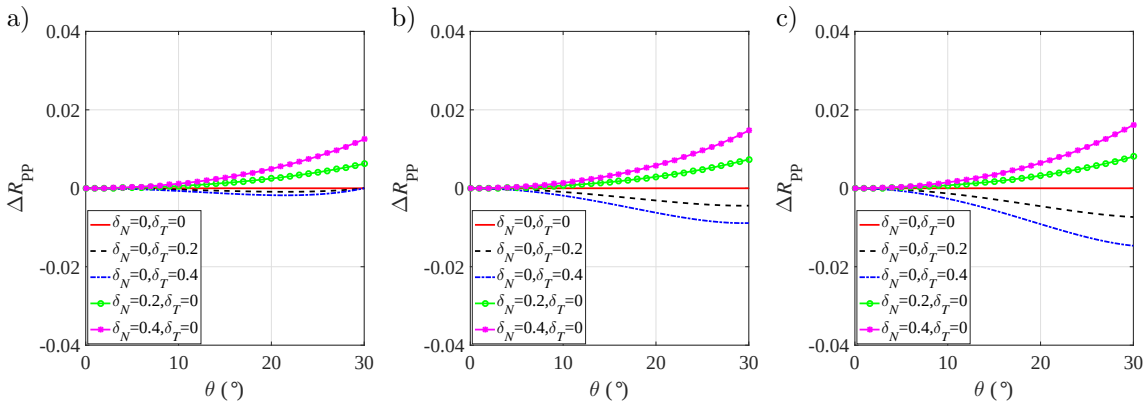

FIG. 4. Effects of fracture weaknesses on differences between azimuthal reflection coefficients. Parameters for computing azimuthal reflection coefficients are $g = 0.25$, $\phi_2 = 90°$ and $\phi_1 = 0°$. a) Tilt angle ν is $60°$; b)Tilt angle ν is $70°$; and c) Tilt angle ν is $80°$.

We observe that the difference between azimuthal reflection coefficients increases with the normal fracture weakness, and decreases as the tangential fracture weakness increases. Comparing Figure 4(a), (b) and (c), we observe that the tilt angle mainly affects the effect of tangential fracture weakness on differences between azimuthal reflection coefficients. It indicates that the effect of tangential fracture weakness on reflection coefficient difference is coupled with the influence of tilt angle, which may induce uncertainties in the estimation of tangential fracture weaknesses. Hence, we consider the tangential fracture weakness (δ_T) and tilted fracture weaknesses ($\delta_{\nu N}$ and $\delta_{\nu T}$) as unknown variables required to be estimated from azimuthal seismic data, which may allow us to implement a linear inversion.

We demonstrate an approach of using azimuthal seismic amplitude differences to estimate unknown parameters (i.e. δ_T, $\delta_{\nu N}$ and $\delta_{\nu T}$). In the case of n reflection interface and

m incidence angle, seismic amplitude difference is generated by

$$\mathbf{d} = \mathbf{G}\mathbf{x}, \tag{13}$$

where

$$\mathbf{d} = \begin{bmatrix} \mathbf{W}\mathbf{R}_{\mathrm{PP}}(\theta_1,\phi_2) - \mathbf{W}\mathbf{R}_{\mathrm{PP}}(\theta_1,\phi_1) \\ \vdots \\ \mathbf{W}\mathbf{R}_{\mathrm{PP}}(\theta_m,\phi_2) - \mathbf{W}\mathbf{R}_{\mathrm{PP}}(\theta_m,\phi_1) \end{bmatrix}_{mn\times 1}, \mathbf{W} = \begin{bmatrix} w_1 & 0 & \dots & 0 \\ w_2 & w_1 & \ddots & \vdots \\ \vdots & \vdots & \ddots & 0 \\ w_n & w_{n-1} & \dots & w_1 \end{bmatrix}_{n\times n}, \mathbf{x} = \begin{bmatrix} \mathbf{R}_{\delta_T} \\ \mathbf{R}_{\delta_{\nu N}} \\ \mathbf{R}_{\delta_{\nu T}} \end{bmatrix}_{3n\times 1},$$

$$\mathbf{R}_{\mathrm{PP}}(\theta,\phi) = \begin{bmatrix} R^1_{\mathrm{PP}}(\theta,\phi) \\ \vdots \\ R^n_{\mathrm{PP}}(\theta,\phi) \end{bmatrix}_{n\times 1}, \mathbf{R}_{\delta_T} = \begin{bmatrix} (\delta_T)_1 \\ \vdots \\ (\delta_T)_n \end{bmatrix}_{n\times 1}, \mathbf{R}_{\delta_{\nu N}} = \begin{bmatrix} (\delta_{\nu N})_1 \\ \vdots \\ (\delta_{\nu N})_n \end{bmatrix}_{n\times 1}, \mathbf{R}_{\delta_{\nu T}} = \begin{bmatrix} (\delta_{\nu T})_1 \\ \vdots \\ (\delta_{\nu T})_n \end{bmatrix}_{n\times 1},$$

$$\begin{aligned} \mathbf{G} &= \begin{bmatrix} \mathbf{A}(\theta_1) & \mathbf{B}(\theta_1) & \mathbf{C}(\theta_1) \\ \vdots & \vdots & \vdots \\ \mathbf{A}(\theta_m) & \mathbf{B}(\theta_m) & \mathbf{C}(\theta_m) \end{bmatrix}_{mn\times 3n}, \mathbf{A}(\theta) = a\sin^2\theta \begin{bmatrix} -g_1 & & \\ & \ddots & \\ & & -g_n \end{bmatrix}_{n\times n}, \\ \mathbf{B}(\theta) &= b\tan^2\theta \begin{bmatrix} -g_1(1-2g_1) & & \\ & \ddots & \\ & & -g_n(1-2g_n) \end{bmatrix}_{n\times n}, \\ \mathbf{C}(\theta) &= b(4\sin^2\theta - \tan^2\theta) \begin{bmatrix} g_1 & & \\ & \ddots & \\ & & g_n \end{bmatrix}_{n\times n}, \end{aligned} \tag{14}$$

in which $a = \cos 2\phi_2 - \cos 2\phi_1$, $b = \cos^2\phi_2 - \cos^2\phi_1$, $w_1, ..., w_n$ are elements of wavelet extracted from input seismic data, and $g_1, ..., g_n$ are average results calculated using S-to-P wave moduli ratios across the corresponding reflection interface.

In order to obtain the tangential fracture weakness and tilted fracture weaknesses, we implement the inversion of azimuthal amplitude differences for the unknown parameter vector **x**. We next propose an approach to constrain the inversion using probabilistic constraints. Following a Bayesian framework, the posterior Probability Distribution function (PDF) is given by (Buland and Omre, 2003)

$$P(\mathbf{x}|\mathbf{d}) \propto P(\mathbf{d}|\mathbf{x})\, P(\mathbf{x}), \tag{15}$$

where $P(\mathbf{x}|\mathbf{d})$ is the posterior PDF, $P(\mathbf{d}|\mathbf{x})$ is the likelihood function, and $P(\mathbf{x})$ is the prior constraint PDF. Under the assumption of Gaussian random noise in observed seismic data, the likelihood function is given by (Downton, 2005)

$$P(\mathbf{d}|\mathbf{x}) = \frac{1}{\sqrt{2\pi\sigma_{\mathrm{e}}^2}} \exp\left[\frac{-(\mathbf{d}-\mathbf{G}\mathbf{x})^{\dagger}(\mathbf{d}-\mathbf{G}\mathbf{x})}{2\sigma_{\mathrm{e}}^2}\right], \tag{16}$$

where σ_{e}^2 is the variance of random noise, and $\dagger$ denotes the transpose of matrix. Following Alemie (2010), we assume the priori constraint follows Cauchy distribution, and the priori constraint PDF is given by

$$P(\mathbf{x}) = \frac{1}{(\pi\sigma_{\mathbf{x}})^{3n}} \exp\left[-\sum_{i=1}^{3n} \ln\left(1 + \frac{{x_i}^2}{\sigma_{\mathbf{x}}^2}\right)\right], \tag{17}$$

where $\sigma_{\mathbf{x}}^2$ represents the variance of unknown parameter vector $\mathbf{x}$, and x_i represents the element of $\mathbf{x}$. Combining equations 15-17, we express the posterior PDF as

$$P\left(\mathbf{x}|\mathbf{d}\right) \propto \frac{1}{\sqrt{2\pi\sigma_{\mathrm{e}}^2}} \frac{1}{\left(\pi\sigma_{\mathbf{x}}\right)^{3n}} \exp\left[J(\mathbf{x})\right], \tag{18}$$

where

$$J(\mathbf{x}) = \frac{(\mathbf{d}-\mathbf{G}\mathbf{x})^{\dagger}(\mathbf{d}-\mathbf{G}\mathbf{x})}{2\sigma_{\mathrm{e}}^2} + \sum_{i=1}^{3n} \ln\left(1+\frac{{x_i}^2}{\sigma_{\mathbf{x}}^2}\right). \tag{19}$$

We next obtain the maximum posterior probability by searching for the minimum of $J(\mathbf{x})$. Differentiating $J(\mathbf{x})$ with respect to $\mathbf{x}$ and letting the resulting expression be zero yields

$$\left(\mathbf{G}^{\dagger}\mathbf{G} + \frac{2\sigma_{\mathrm{e}}^2}{\sigma_{\mathbf{x}}^2 + x_i^2}\right)\mathbf{x} = \mathbf{G}^{\dagger}\mathbf{d}. \tag{20}$$

The iterative re-weighted least squares(IRLS) algorithm, which is proposed by Daubechies et al. (2010) and Alemie (2010), is employed to solve the inversion problem.

RESULTS

Synthetic examples: Stability and robustness verification

Well log model

We first use a well log model to generate synthetic seismic amplitude differences, and then we implement the inversion for the tangential fracture weaknesses and tilted fracture weaknesses to verify the stability and robustness of the proposed inversion approach. In Figure 5(a) we plot curves of P- and S-wave velocities (V_{P} and V_{S}), density ρ, and fracture density e, and in Figure 5(b) we plot the model of tilt angle ν and the computed tangential fracture weakness and tilted fracture weaknesses computed using expressions of dry fracture weaknesses (Chen et al., 2018).

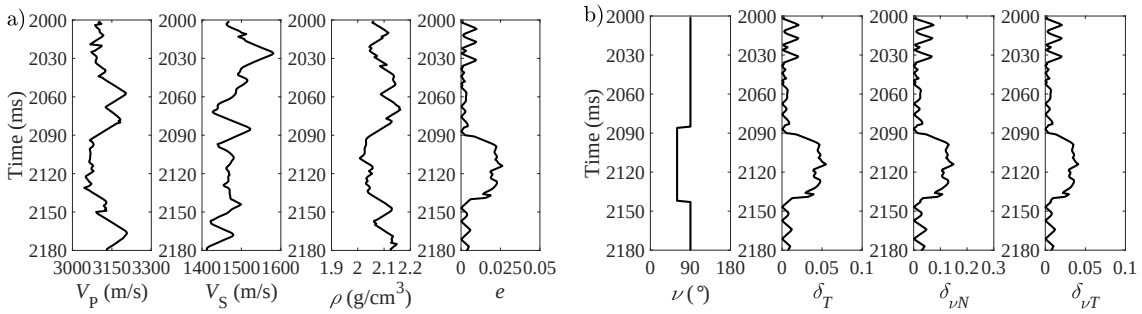

FIG. 5. A well log model. a) Curves of P- and S-wave velocities, density and fracture density; and b) the model of of tilt angle and the computed tangential fracture weakness and tilted fracture weaknesses.

Using equation 13, we generate synthetic seismic amplitude differences utilizing a 35Hz Ricker wavelet, and azimuthal angles ϕ_1 and ϕ_2 are 0° and 90°. Figure 6(a)-6(c)

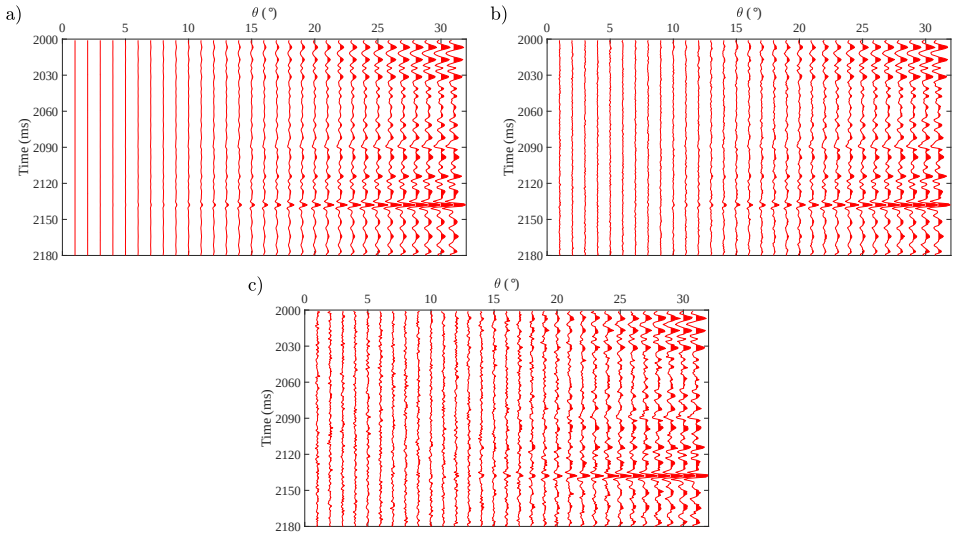

FIG. 6. Synthetic seismic amplitude differences. (a) No noise; (b) SNR=5; and (c) SNR=2.

plot the generated seismic amplitude differences in the case of no noise and signal-to-ratio (SNR) of 5 and 2. We observe that seismic amplitude differences mainly exist at the middle and large incidence angles ($15^\circ \leq \theta \leq 30^\circ$), which is essentially in agreement with the variation of reflection coefficient difference with incidence angle. It indicates that in order to estimate the tangential fracture weakness and tilted fracture weaknesses, we should employ azimuthal seismic amplitude differences of middle and large incidence angles as much as possible. We next employ the generated seismic amplitude differences (the incidence angle range 15°-30°) to estimate the tangential fracture weakness and tilted fracture weaknesses. Comparisons between true and inversion values of tangential fracture weakness and tilted fracture weaknesses are plotted in Figure 7(a)-7(d). From Figure 7(a), we

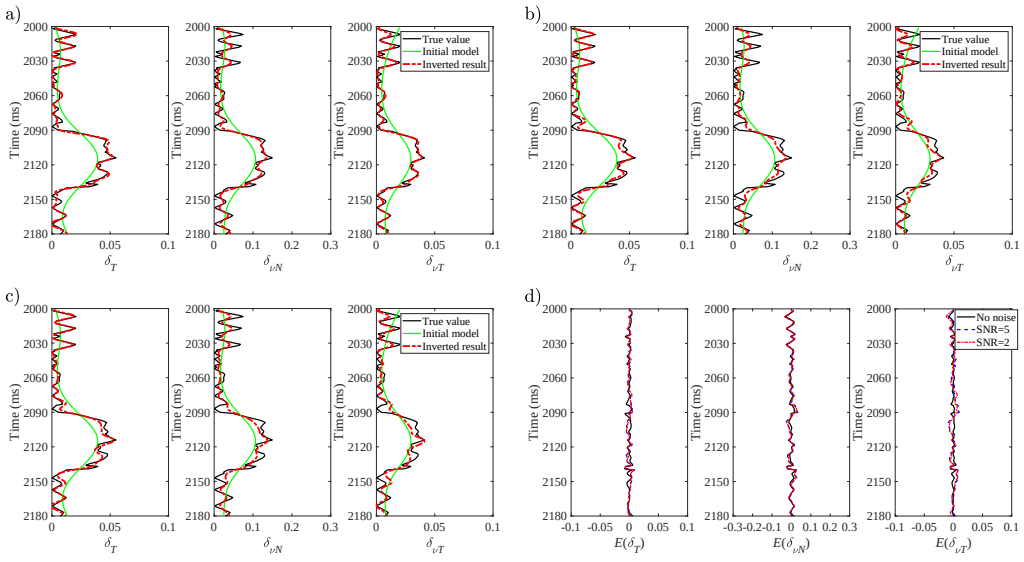

FIG. 7. Comparisons between true values and inversion results of tangential fracture weakness and tilted fracture weaknesses. a) No noise; b) SNR=5; c) SNR=2; and d) Errors between inversion results and true values, e.g. $E(\delta_T) = Inv(\delta_T) - True(\delta_T)$, $True(\delta_T)$ is the true value of δ_T, and $Inv(\delta_T)$ is the inversion result of δ_T. Green curve represents the initial model of unknown parameter, which is the smoothed version of true value.

observe that the unknown parameters are estimated correctly in the case of no noise being added into synthetic data; From Figure 7(b)-7(c), we see that there is a good match between inversion results and true values in the case of seismic data being added with a moderate noise (i.e. $\mathrm{SNR} \geq 2$); and Figure 7(d) plots errors between true values and inversion results, which fluctuate near zero. We conclude that tests on synthetic data confirm the stability and robustness of the proposed inversion approach.

2D overthrust model

We proceed to the verification of robustness and stability of the proposed approach using a 2D overthrust model. P- and S-wave velocities and density are plotted in Figure 8(a); in Figure 8(b), we plot a model of fracture density e, in which we assume there are four fractured layers, and we compute the normal and tangential fracture weaknesses (δ_N and δ_T) again using expressions of dry fracture weaknesses (Chen et al., 2018). Assuming the fractured layers have different tilt angles, we calculate tilted fracture weaknesses ($\delta_{\nu N}$ and $\delta_{\nu T}$), as plotted in Figure 8(c). Using a 35 Hz Ricker wavelet, we generate synthetic seismic

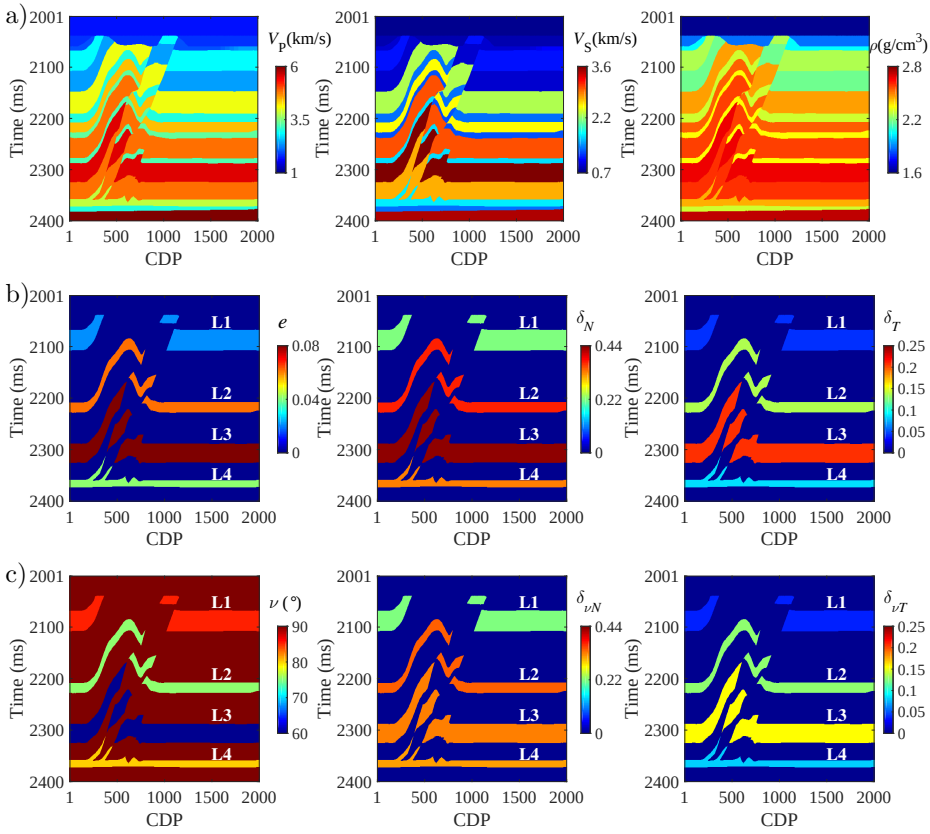

FIG. 8. a) P- and S-wave velocities and density of overthrust model; b) Model of fracture density, and computed fracture weaknesses δ_N and δ_T; c) Model of tilt angles, and calculated tilted fracture weaknesses $\delta_{\nu N}$ and $\delta_{\nu T}$.

amplitude differences based on equation 13, and we also add Gaussian random noise (SNR of 2) into the synthetic seismic data. Utilizing the noisy seismic data, we implement the inversion for the tangential fracture weakness and tilted fracture weaknesses for each CDP of the overthrust model. Figure 9(a) plots initial models of δ_T, $\delta_{\nu N}$ and $\delta_{\nu T}$ used in the

inversion, which are the smoothed version of the corresponding true value; and in Figure 9(b), we plot the inversion results of unknown parameters. Figure 9(c) plots comparisons between true values (blue curves) and inversion results (red curves) of tangential fracture weakness and tilted fracture weaknesses at CDP 500.

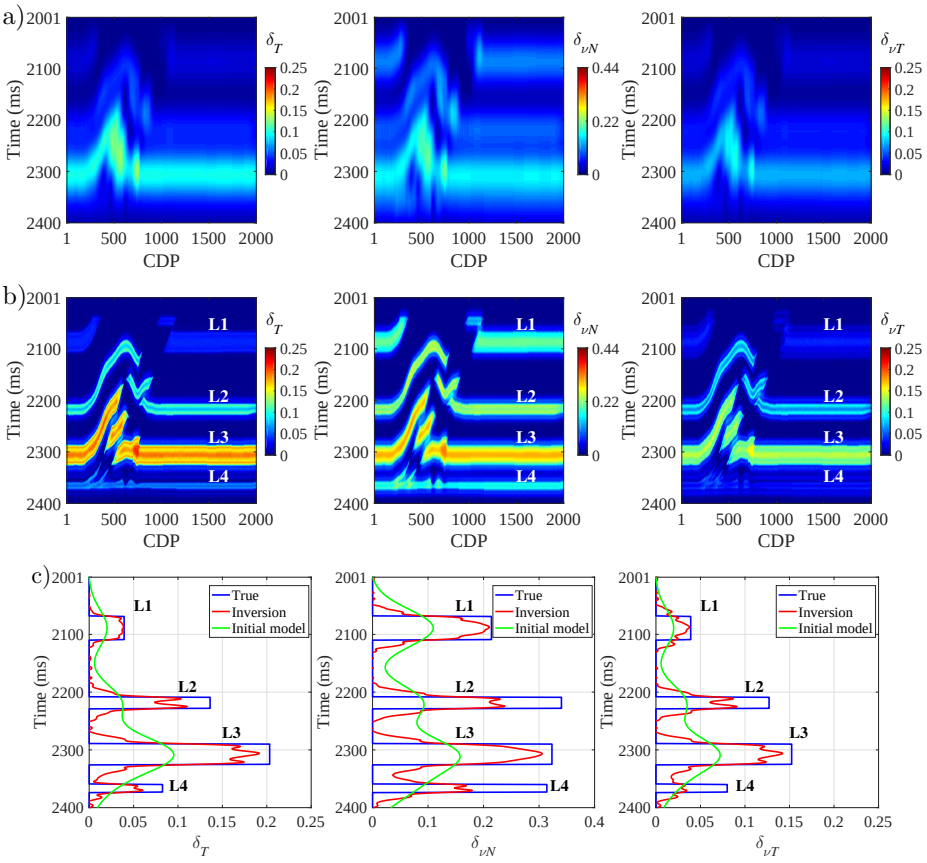

FIG. 9. a) Initial models used in the inversion; b) Inversion results of tangential fracture weakness and tilted fracture weaknesses. The initial model is a smoothed version of true value; and c) Comparisons between inversion result and true value, and green curves represent the initial model.

Comparing true values plotted in Figure 8 and inversion results shown in Figure 9, we observe that the tangential fracture weakness δ_T and tilted normal fracture weakness $\delta_{\nu N}$ of fractured layers L1, L2, L3 and L4 are predicted stably and reliably even in the case of SNR of 2. From the inversion result of $\delta_{\nu T}$, we may obtain reliable results for fractured layers L2 and L3; however, the accuracy of inversion for layer L1 and L4 should be improved.

Real data example

We proceed to applying the proposed approach to a real data set to further confirm its feasibility. The data are acquired over a fractured carbonate rock reservoir, and they have been sorted to common azimuth gathers and transferred from offset domain to incidence angle domain for each azimuth sector. It is important to stress that the processing is implemented by the institute who provides us the data. In Figure 10(a), we plot seismic angle gathers along azimuths $\phi_1 = 30°$ and $\phi_2 = 150°$ and differences between the angle gathers

at the location of CDP 195; in Figure 10(b), we also show stacked seismic profiles along azimuths ϕ_1 and ϕ_2 and differences between stacked seismic profiles. The ellipse in the figure indicates the location of the fractured reservoir.

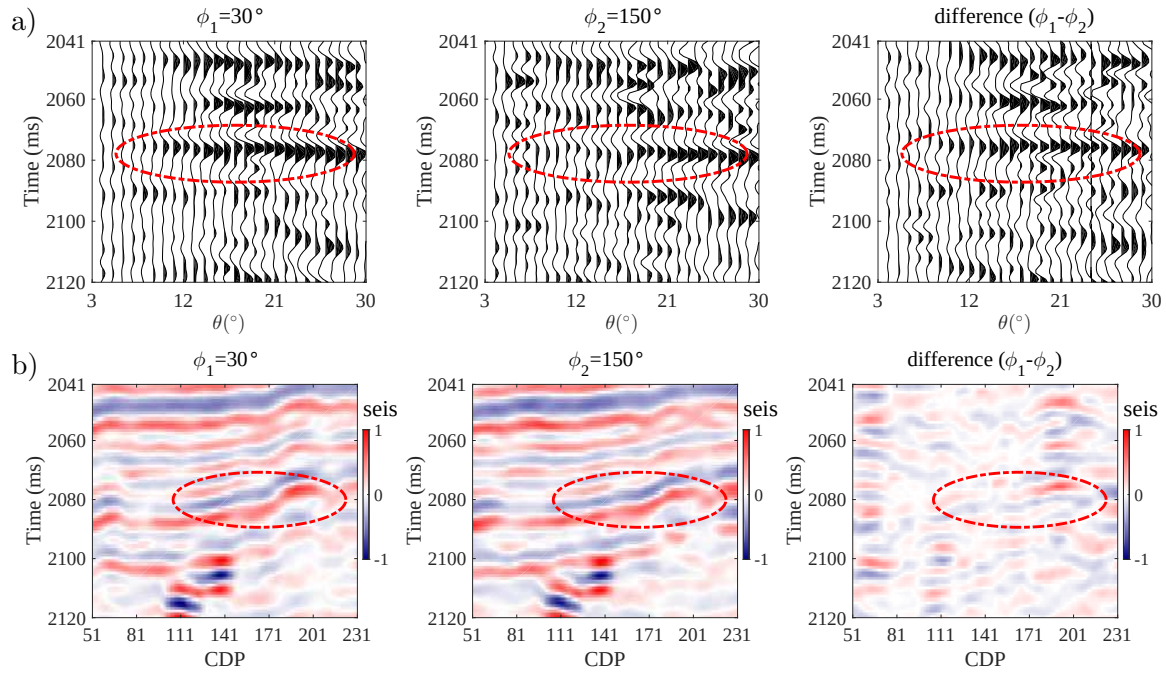

FIG. 10. a) Seismic angle gathers along two different azimuths $\phi_1 = 30°$ and $\phi_2 = 150°$, and differences between these two azimuthal angle gathers; b) Stacked seismic profiles at azimuths ϕ_1 and ϕ_2, and differences between stacked seismic data.

From Figure 10(a) and 10(b), we observe that a strong reflection amplitude exhibits at the location of the fractured reservoir in both the angle gather and the stacked data, and there are also large amplitude residuals at the location of the fractured reservoir. We next use seismic angle gather differences to implement the inversion for the tangential fracture weakness and tilted fracture weaknesses using the proposed inversion approach. We first plot constructed initial models of unknown parameters in Figure 11. The method to construct initial models is presented in Discussion section.

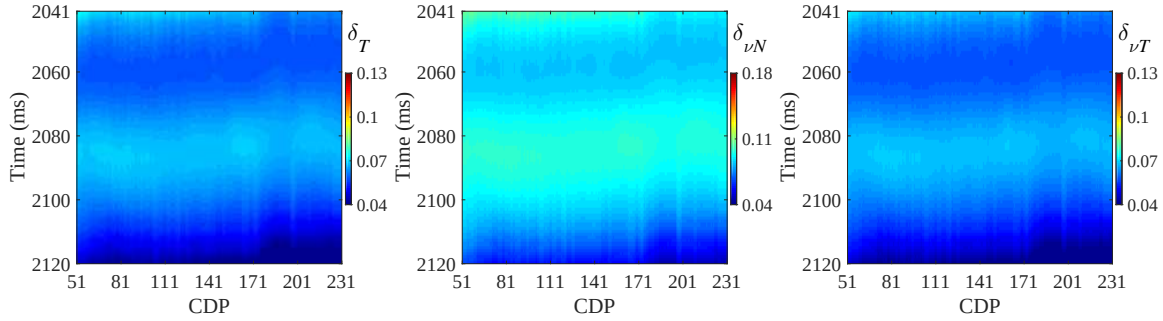

FIG. 11. Initial models of tangential fracture weakness and tilted fracture weaknesses.

Figure 12 plots inversion results of tangential fracture weakness and tilted fracture weaknesses. We observe that at the location of fractured reservoir marked by the ellipse, the

tangential fracture weakness and tilted fracture weaknesses exhibit relatively large values. Comparing the inverted tangential fracture weakness δ_T and the estimated tilted tangential fracture weakness $\delta_{\nu T}$, we see that there is an apparent difference between inversion results of δ_T and $\delta_{\nu T}$ at the location of fractured reservoir, which reveals that the fractures are tilted.

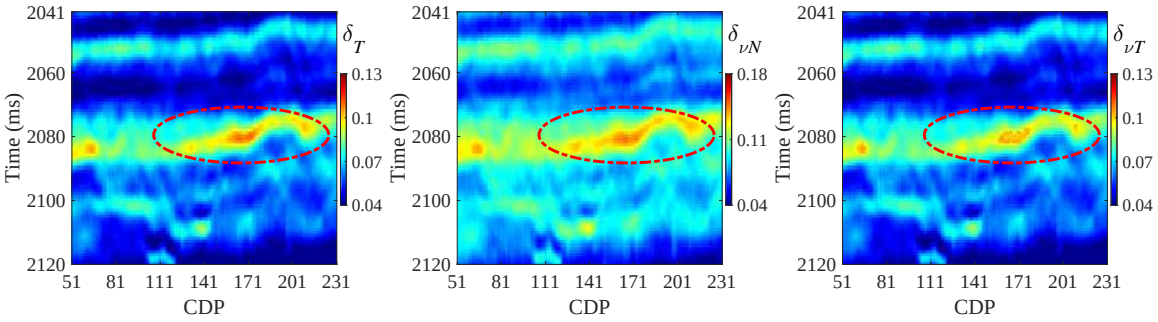

FIG. 12. Inversion results of tangential fracture weakness and tilted fracture weaknesses.

Using the inversion results of δ_T and $\delta_{\nu T}$, we may compute values related to tilt angle (i.e. $\sin^2 \nu$), as plotted in Figure 13. We observe that the computed result shows a relatively low value at the fractured reservoir, which again confirms the fractures in the reservoir are tilted.

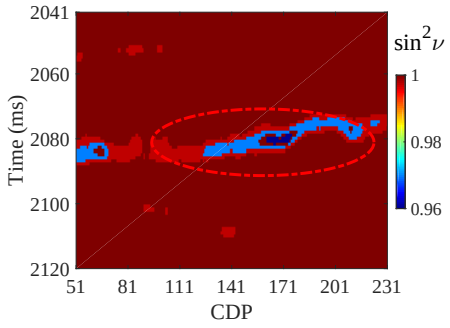

FIG. 13. Computed results related to tilt angles of fractures (i.e. $\sin^2 \nu$).

DISCUSSIONS

We derive a linearized reflection coefficient in terms of fracture weaknesses for titled transversely isotropic (TTI) media. Based on the derived reflection coefficient, we demonstrate a stable approach to estimate the tangential fracture weakness and tilted fracture weaknesses from azimuthal seismic amplitude differences. Some assumptions should be satisfied while using the derived reflection coefficient and the proposed inversion approach, which involve:

1) The derived reflection coefficient is applicable to the case of the reflection interfaces separating one isotropic medium and a tilted fracture medium, which means the overlying and underlying media of fractured reservoirs are approximately isotropic;

2) The layer only contains one set of parallel and tilted fractures. The tilt angle of fractures is relatively high because the accuracy of derived reflection coefficient is acceptable in the case of $\nu \geq 60^\circ$, and the fractured layer has a small fracture density (i.e., $e \leq 0.2$). In addition, we assume the tilt angle of non-fractured layers to be 90°;

3) The maximum incidence angle of input seismic data employed to implement the proposed inversion for tilted fracture weaknesses is around 30°.

Initial models of unknown parameters are required in the proposed inversion approach. For synthetic examples, we use the smoothed version of true value as the initial model. Here we discuss how to construct initial models while applying the inversion approach to real data. Rüger (1998) proposed PP-wave linearized reflection for HTI media, and Bachrach et al. (2009) presented two-term reflection coefficient based on Rüger's equation

$$R_{\mathrm{PP}}(\theta,\phi) = I + U\sin^2\theta = I + \left(U_{\mathrm{iso}} + U_{\mathrm{ani}}\cos^2\phi\right)\sin^2\theta, \tag{21}$$

where I is Amplitude-Versus-Offset (AVO) intercept, U is AVO gradient, and U_{iso} and U_{ani} are isotropic and anisotropic parts of AVO gradient, respectively. Chen et al. (2017) expressed the anisotropic part of AVO gradient in terms of fracture weaknesses

$$U_{\mathrm{ani}} = -g\left(1-2g\right)\delta_N + g\delta_T. \tag{22}$$

We first employ azimuthal seismic data to implement the estimation of AVO intercept and gradient using a commercial software package. Using equation 21, we may compute the anisotropic part of AVO gradient. Again using the commercial software package, we estimate P- and S-wave velocity from input seismic data to compute the S-to-P wave moduli ratio g. For dry fractures, the relationship between the normal and tangential fracture weaknesses is given by

$$\delta_N = \frac{3-2g}{4g\left(1-g\right)}\delta_T. \tag{23}$$

Substituting equation 23 into equation 22, we may compute the normal fracture weakness using the estimated results of anisotropic part of AVO gradient and S-to-P moduli ratio, and then we calculate the tangential fracture weakness. The smoothed version of tangential fracture weakness is used as initial models of both δ_T and $\delta_{\nu T}$, and the smoothed version of normal fracture weakness is used as initial model of $\delta_{\nu N}$.

CONCLUSIONS

Based on the stiffness matrix of horizontal transversely isotropic (HTI) media proposed by the linear slip model, we express the stiffness matrix of tilted transversely isotropic (TTI) media in terms of tilted fracture weaknesses. Using perturbations in stiffness parameters in the case of an interface separating an isotropic layer and a TTI layer, we derive a linearized reflection coefficient in terms of tilted fracture weaknesses. Based on the derived reflection coefficient, we propose a stable inversion approach to employ amplitude differences between azimuthal seismic data to estimate tangential fracture weakness (δ_T), tilted normal fracture weakness ($\delta_{\nu N}$) and tilted tangential fracture weakness ($\delta_{\nu T}$). Applying

the proposed inversion approach to synthetic seismic data generated using a well log model and a 2D overthrust model respectively, we conclude that the unknown parameter vector involving the tangential fracture weakness and titled fracture weaknesses is estimated stably and reliably in the case of synthetic data containing a moderate noise/error (SNR$\geq$2). A test on a real data set acquired over a fractured carbonate reservoir reveals that the proposed inversion method may provide realistic and meaningful results of tangential fracture weakness and tilted fracture weaknesses. Combining the estimated tangential fracture weakness and tilted tangential fracture weakness, we may compute the tilt angle of fractures, which can guide more accurate fracture characterization in unconventional reservoirs. Therefore, the proposed inversion approach has been demonstrated to implement interpretable and verifiable predictions, and it appears to be an additional tool for detecting tilted natural fractures.

ACKNOWLEDGMENTS

The industrial sponsors of the Consortium for Research in Elastic Wave Exploration Seismology (CREWES) are thanked for their support. We gratefully acknowledge additional support from Natural Science and Engineering Research Council of Canada through the grant no. CRDPJ 461179-13. This research was undertaken thanks in part to funding from the Canada First Research Excellence Fund, and the Mitacs Accelerate grant *Responsible Development of Unconventional Hydrocarbon Reserves*. The SINOPEC Key Lab of Multi-Component Seismic Technology is thanked for providing the processed real data. Hampson-Russell software was used for the estimation of AVO intercept and gradient and P- and S-wave velocities.

REFERENCES

Aki, K., and Richards, P. G., 2002, Quantitative seismology: University science books.

Alemie, W. M., 2010, Regularization of the avo inverse problem by means of a multivariate cauchy probability distribution: M.Sc. thesis.

Alkhalifah, T., 1995, Efficient synthetic-seismogram generation in transversely isotropic, inhomogeneous media: Geophysics, **60**, No. 4, 1139–1150.

Alkhalifah, T., and Larner, K., 1994, Migration error in transversely isotropic media: Geophysics, **59**, No. 9, 1405–1418.

Auld, B. A., 1990, Acoustic fields and waves in solids: Krieger, Florida.

Avseth, P., Mukerji, T., and Mavko, G., 2010, Quantitative seismic interpretation: Applying rock physics tools to reduce interpretation risk: Cambridge university press.

Bachrach, R., Sengupta, M., Salama, A., and Miller, P., 2009, Reconstruction of the layer anisotropic elastic parameters and high-resolution fracture characterization from p-wave data: A case study using seismic inversion and bayesian rock physics parameter estimation: Geophysical prospecting, **57**, No. 2, 253–262.

Bakulin, A., Grechka, V., and Tsvankin, I., 2000, Estimation of fracture parameters from reflection seismic data–part i: Hti model due to a single fracture set: Geophysics, **65**, No. 6, 1788–1802.

Bakulin, A., Woodward, M., Nichols, D., Osypov, K., and Zdraveva, O., 2010, Building tilted transversely isotropic depth models using localized anisotropic tomography with well information: Geophysics, **75**, No. 4, D27–D36.

Behera, L., and Tsvankin, I., 2009, Migration velocity analysis for tilted transversely isotropic media: Geophysical Prospecting, **57**, No. 1, 13–26.

Berryman, J. G., Grechka, V. Y., and Berge, P. A., 1999, Analysis of thomsen parameters for finely layered vti media: Geophysical Prospecting, **47**, No. 6, 959–978.

Buland, A., and Omre, H., 2003, Bayesian wavelet estimation from seismic and well data: Geophysics, **68**, No. 6, 2000–2009.

Carcione, J. M., 1992, Anisotropic q and velocity dispersion of finely layered media: Geophysical Prospecting, **40**, No. 7, 761–783.

Carcione, J. M., 2000, A model for seismic velocity and attenuation in petroleum source rocks: Geophysics, **65**, No. 4, 1080–1092.

Chen, H., Ji, Y., and Innanen, K. A., 2018, Estimation of modified fluid factor and dry fracture weaknesses using azimuthal elastic impedance: Geophysics, **83**, No. 1, WA73–WA88.

Chen, H., Zhang, G., Chen, J., and Yin, X., 2014, Fracture filling fluids identification using azimuthally elastic impedance based on rock physics: Journal of Applied Geophysics, **110**, 98–105.

Chen, H., Zhang, G., Ji, Y., and Yin, X., 2017, Azimuthal seismic amplitude difference inversion for fracture weakness: Pure and Applied Geophysics, **174**, No. 1, 279–291.

Daubechies, I., DeVore, R., Fornasier, M., and Güntürk, C. S., 2010, Iteratively reweighted least squares minimization for sparse recovery: Communications on Pure and Applied Mathematics: A Journal Issued by the Courant Institute of Mathematical Sciences, **63**, No. 1, 1–38.

Downton, J. E., 2005, Seismic parameter estimation from avo inversion: Ph.D. thesis, University of Calgary.

Fletcher, R. P., Du, X., and Fowler, P. J., 2009, Reverse time migration in tilted transversely isotropic (tti) media: Geophysics, **74**, No. 6, WCA179–WCA187.

Grechka, V., Pech, A., Tsvankin, I., and Han, B., 2001, Velocity analysis for tilted transversely isotropic media: A physical modeling example: Geophysics, **66**, No. 3, 904–910.

Gurevich, B., 2003, Elastic properties of saturated porous rocks with aligned fractures: Journal of Applied Geophysics, **54**, No. 3, 203–218.

Hudson, J., 1980, Overall properties of a cracked solid: Mathematical Proceedings of the Cambridge Philosophical Society, **88**, No. 2, 371–384.

Nadri, D., Sarout, J., Bóna, A., and Dewhurst, D., 2012, Estimation of the anisotropy parameters of transversely isotropic shales with a tilted symmetry axis: Geophysical Journal International, **190**, No. 2, 1197–1203.

Pšenčík, I., and Gajewski, D., 1998, Polarization, phase velocity, and nmo velocity of qp-waves in arbitrary weakly anisotropic media: Geophysics, **63**, No. 5, 1754–1766.

Pšenčík, I., and Vavryčuk, V., 1998, Weak contrast pp wave displacement r/t coefficients in weakly anisotropic elastic media: Pure and Applied Geophysics, **151**, No. 2-4, 699–718.

Rüger, A., 1996, Reflection coefficients and azimuthal avo analysis in anisotropic media.: Ph.D. thesis, Colorado School of Mines.

Rüger, A., 1998, Variation of p-wave reflectivity with offset and azimuth in anisotropic media: Geophysics, **63**, No. 3, 935–947.

Schoenberg, M., and Douma, J., 1988, Elastic wave propagation in media with parallel fractures and aligned cracks: Geophysical Prospecting, **36**, No. 6, 571–590.

Schoenberg, M., and Protázio, J., 1992, ′zoeppritz′rationalized and generalized to anisotropy: Journal of seismic exploration, **1**, No. S1, 125–144.

Schoenberg, M., and Sayers, C. M., 1995, Seismic anisotropy of fractured rock: Geophysics, **60**, No. 1, 204–211.

Shaw, R. K., and Sen, M. K., 2006, Use of avoa data to estimate fluid indicator in a vertically fractured medium: Geophysics, **71**, No. 3, C15–C24.

Sheriff, R. E., and Geldart, L. P., 1995, Exploration seismology: Cambridge university press.

Shragge, J., 2016, Acoustic wave propagation in tilted transversely isotropic media: Incorporating topography: Geophysics.

Shuey, R., 1985, A simplification of the zoeppritz equations: Geophysics, **50**, No. 4, 609–614.

Stovas, A., and Alkhalifah, T., 2013, Mapping of moveout in tilted transversely isotropic media: Geophysical Prospecting, **61**, No. 6, 1171–1177.

Stovas, A., Landrø, M., and Avseth, P., 2006, Avo attribute inversion for finely layered reservoirs: Geophysics, **71**, No. 3, C25–C36.

Thomsen, L., 1986, Weak elastic anisotropy: Geophysics, **51**, No. 10, 1954–1966.

Thomsen, L., 1988, Reflection seismology over azimuthally anisotropic media: Geophysics, **53**, No. 3, 304–313.

Tsvankin, I., 1997, Anisotropic parameters and p-wave velocity for orthorhombic media: Geophysics, **62**, No. 4, 1292–1309.

Wang, H., and Peng, S., 2015, Reflection coefficient of qp, qs and sh at a plane boundary between viscoelastic tti media: Geophysical Journal International, **204**, No. 1, 555–568.

Wang, X., and Tsvankin, I., 2013, Ray-based gridded tomography for tilted transversely isotropic media: Geophysics.